Structure, magnetization, and NMR studies of the spin-glass compound $(Li_xV_{1-x})_3BO_5$ ($x \approx 0.40$ and 0.33)

X. Zong, A. Niazi, F. Borsa, X. Ma,* and D. C. Johnston
Ames Laboratory and Department of Physics and Astronomy, Iowa State University, Ames, Iowa 50011, USA
(Received 22 November 2006; revised manuscript received 12 June 2007; published 31 August 2007)

Structural and magnetic properties of $(Li_xV_{1-x})_3BO_5$ powders ($x=0.33$) and single crystals ($x=0.40$) were studied by x-ray diffraction, magnetization, and NMR measurements. Both powder and single crystal x-ray diffraction data are consistent with the previously reported structure of the system. Magnetization measurements show an overall antiferromagnetic interaction among vanadium spins and reveal a transition into a spin glass state at a sample and magnetic field dependent temperature below ~10 K. The high temperature ($T > 20$ K) susceptibility is analyzed using a linear spin trimer model suggested in the literature but such a model is found to be insufficient to explain the data. ^{7}Li and ^{11}B NMR studies indicate an inhomogeneous dynamics close to the zero-field spin-glass transition temperature. The distribution of electronic spin relaxation times is derived using a recently proposed method and the broad temperature-dependent distribution obtained gives a consistent description of the NMR results. The temperature dependence of the distribution indicates a strong slowing down of the local moment spin dynamics as the system cools toward the zero-field spin-glass transition temperature even in the presence of a strong applied magnetic field up to 4.7 T.

DOI: 10.1103/PhysRevB.76.054452 PACS number(s): 76.60.−k, 75.50.Lk, 75.40.Cx, 75.20.Ck

I. INTRODUCTION

Spin glasses have attracted continuous research interest for more than 30 years. However, some fundamental questions remain controversial. For example, recent debate focuses on whether an isotropic three-dimensional Edward-Anderson Heisenberg spin glass has a finite transition temperature.[1–6] Another important question concerns whether a spin-glass transition can occur in a finite magnetic field. An answer to this second question would allow one to distinguish between two main scenarios concerning the nature of the spin-glass phase; the "droplet"[7] and "replica symmetry breaking"[8] scenarios. Magnetization measurements on the Ising spin glass $Fe_xMn_{1-x}TiO_3$ indicated that the spin-glass state is destroyed by a nonzero magnetic field and lend support to the droplet picture.[9–11] On the other hand, the persistence of a frozen spin-glassy phase in an applied magnetic field in different Heisenberg systems that show spin-glass transitions in zero field was inferred through magnetization and torque measurements.[12–15]

The origin of the nonexponential spin autocorrelation functions[16–18] in spin glasses is also an issue of continuous debate. It was often assumed that the nonexponential correlation function arises from the sum of a distribution of single exponential correlation functions of different magnetic entities in the system. Under such an assumption, a distribution of relaxation times could be derived from muon spin depolarization, magnetization, and neutron spin-echo experiments.[16,19–21] Such a viewpoint was supported by numerical simulations, which showed that the spin autocorrelation functions are spatially inhomogeneous close to the spin-glass transition temperature.[22–24] Another viewpoint claims that the nonexponential spin autocorrelation function is an intrinsic, homogeneous feature of spin glasses.[18,25] One argument to support such a view is that the different relaxation times are associated with different excitation modes in the system that overlap in space. Since a spin can take part in different modes simultaneously, the relaxation for each spin is nonexponential.[25] An additional homogeneous relaxation mechanism is hierarchical relaxation where the relaxation pathway at a specific time depends on relaxation occurring in previous pathways.[26]

$(Li_xV_{1-x})_3BO_5$ is a Heisenberg spin-glass system first synthesized and studied by Onoda.[27] It has an orthorhombic crystal structure (space group *Pbam*), as shown in Fig. 1, where Li and V statistically occupy to varying extent four inequivalent sites VL1-VL4 that are octahedrally coordinated by oxygen atoms. Transport studies in the temperature region between 80 and 300 K showed insulating behavior. The high

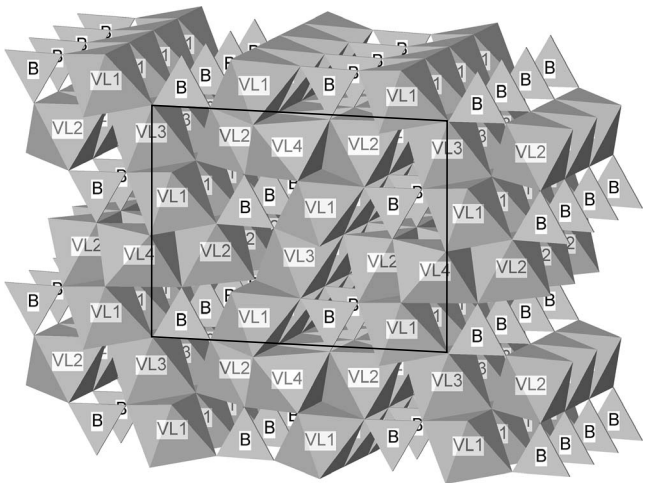

FIG. 1. The crystal structure of $(Li_xV_{1-x})_3BO_5$. B represents boron sites and VL1–VL4 are the four sites occupied by vanadium or lithium atoms. Oxygen atoms occupy the vertices of the triangles and octahedra. The rectangle indicates the size of a unit cell in the plane of the page. The crystallographic *a* and *b* axes are along the vertical and horizontal directions in the plane of the page, respectively. The *c* axis is perpendicular to the page.

temperature magnetic susceptibility χ followed the Curie-Weiss law with a negative Weiss temperature, indicating an overall antiferromagnetic interaction among vanadium magnetic moments. The magnetization M deviates from being proportional to the applied magnetic field H at temperatures $T<25$ K and a transition to a spin-glass state at lower T was suggested.[27] The inverse magnetic susceptibility $\chi^{-1}(T)$ data showed negative curvature below ~100 K [see also Fig. 3(a) below], which was attributed by Onoda to the occurrence of antiferromagnetic clusters or spin trimers.[27] However, additional experimental studies are necessary to further characterize the magnetic state of the system at low temperatures.

In this paper, we report further structure, magnetization, and NMR studies of the compound $(Li_xV_{1-x})_3BO_5$. The crystal structure in Ref. 27 is confirmed by x-ray diffraction studies on powder and single crystal samples. In particular, the presence of disorder and frustration, the two ingredients usually considered necessary for a spin-glass state, will be discussed. A study of the linear spin trimer model suggested by Onoda will be carried out and compared with the high temperature susceptibility results. The low temperature spin-glass state is confirmed by the presence of magnetic irreversibility, slow relaxation of thermal remnant magnetization, and memory and rejuvenation effects. Furthermore, we also study the effect of magnetic field on the spin-glass behavior by measuring the change of magnetization irreversibility as a function of magnetic field strength. It is found that the onset of irreversibility is suppressed to lower temperature at higher magnetic field.

NMR has proved a useful microscopic tool to study the local spin dynamics in spin-glass systems.[28–32] In recent NMR studies in heavy fermion LiV_2O_4 containing a small amount of magnetic defects (~0.73 mol %), we found a stretched exponential behavior $1-M(t)/M(\infty)=\exp[-(t/T_1^*)^\beta]$ for the recovery of the ^{7}Li nuclear magnetization versus time $M(t)$ following a saturation pulse sequence in the temperature range 0.5–4.2 K.[33] Earlier μSR studies showed that LiV_2O_4 with 0.13 mol % magnetic defects undergoes a spin-glass freezing below ~0.7 K.[34] The stretched exponential recovery is in strong contrast to a single exponential behavior observed in pure LiV_2O_4 samples, where no spin-glass behavior was observed down to 20 mK. In order to better understand the relation between the stretched exponential recovery and the dynamics in spin glasses, it is highly desirable to study the nuclear spin-lattice relaxation behavior in other spin-glass systems. We have found that the ^{7}Li nuclear spin lattice relaxation in $(Li_{0.33}V_{0.67})_3BO_5$ indeed follows a temperature-dependent stretched exponential behavior.

It was previously shown[33,35] that a unique distribution of nuclear spin-lattice relaxation rates $1/T_1$'s can be obtained from the observed stretched exponential recovery with given fitted values of $1/T_1^*$ and β. In this paper, by assuming the presence of dynamical heterogeneity in the system, we derive the temperature-dependent distribution of the vanadium electronic spin relaxation times from the ^{7}Li relaxation data. Our NMR results reveal the persistence of a continuous broadening and dramatic slowing down of the electronic spin dynamics even under a strong (4.7 T) magnetic field as the *zero-field* spin-glass transition temperature is approached, in strong contrast to the magnetization results which show a suppression of the long range spin-glass transition in a field.

This paper is organized as follows. Experimental details are presented in Sec. II. The results of our structural studies are given in Sec. III. Magnetization and NMR studies are presented in Secs. IV and V, respectively. In Sec. VI, we conclude the paper with a summary and discussion of the main results.

II. EXPERIMENT

Crystals of $(Li_xV_{1-x})_3BO_5$ were grown under high purity argon gas flow with a flux consisting of $LiBO_2$ (4 *N*, Alfa Aesar) and LiV_2O_4 with molar ratio 14.5:1. The x value is 0.4, as determined from the refinement below of the single crystal x-ray diffraction pattern. The mixture was contained in a platinum crucible and soaked at 1100 °C for 48 h, then cooled at 1 °C/h to 825 °C at which point the furnace was turned off to cool. The flux was removed by dissolving in hot water at 80 °C. The typical dimensions of the crystals were $0.3\times0.3\times6$ mm^3. LiV_2O_4 was prepared using standard solid state reaction. The starting materials were Li_2CO_3 (5 *N*, Alfa Aesar), V_2O_5 (4 *N*, MV Laboratory), and V_2O_3 (4 *N*, MV Laboratory). Details of the LiV_2O_4 synthesis procedure are described in Ref. 36. We note that this crystal growth method is different from that used in Ref. 27, where the flux instead consisted of $LiBO_2$ and $LiVO_2$.

The polycrystalline samples of $(Li_xV_{1-x})_3BO_5$ were made from a mixture of V_2O_3 (4 *N*, MV Laboratory) and $LiBO_2$ (4 *N*, Alfa Aesar) with molar ratio 1:1. The nominal composition was $(Li_{0.33}V_{0.67})_3BO_5$. The mixture of starting materials was ground and pelletized and then sealed inside a quartz tube under vacuum. It was then heated at 800 °C for 4 days and then air quenched to room temperature.

Single crystal x-ray diffraction measurements were carried out on a Bruker SMART diffractometer with a graphite monochromator and Mo $K\alpha$ radiation at $T=293(2)$ K. The x-ray powder diffraction data were obtained at room temperature using a Rigaku Geigerflex diffractometer with a curved graphite crystal monochromator and Cu $K\alpha$ radiation. The 2θ scan range was 10°–90° with 0.02° step size. Full profile Rietveld analyses on the powder x-ray diffraction pattern were carried out using EXPGUI,[37] a graphical user interface for GSAS.[38]

Magnetization measurements were carried out using a Quantum Design superconducting quantum interference device magnetometer in the temperature T range 1.8–350 K and applied magnetic field H range 0–5.5 T. The crystals were aligned along the crystallographic c axis using Duco cement (a and b axes randomly oriented) on a plastic film. The Duco cement and the plastic film are diamagnetic and contribute less than 2% to the total magnetization. Their contributions were subtracted to obtain the sample magnetization.

^{7}Li and ^{11}B NMR measurements were performed on the powder sample $(Li_{0.33}V_{0.67})_3BO_5$ in the T range 1.5–295 K. The typical saturation recovery sequence was used for nuclear spin lattice relaxation measurements. Spin-spin re-

laxation rates were measured by varying the separation between $\pi/2$ and π pulses which generated an echo. The typical $\pi/2$ pulse length was 3 μs. ^{7}Li NMR spectra were measured at $H=3$ T. The spectra with narrow full width at half maximum (FWHM) intensity $\leqslant 100$ kHz were obtained via the Fourier transform of half the echo signal, while broader spectra were measured by sweeping the rf frequency and recording the echo area at each point.

III. CRYSTAL STRUCTURE

X-ray diffraction studies confirm that both our single crystal and polycrystalline samples have the same structure and approximately the same composition as reported in Ref. 27 ($x=0.31, 0.33$). The system has an orthorhombic crystal structure (space group *Pbam*), as shown in Fig. 1, where Li or V occupy four inequivalent sites VL1-VL4 in each unit cell that are octahedrally coordinated by oxygen atoms.

The single crystal x-ray diffraction data were collected in the Miller index ranges of $-12 \leqslant h \leqslant 12$, $-16 \leqslant k \leqslant 16$, and $-3 \leqslant l \leqslant 3$. A total of 2887 reflections were observed, among which 464 are independent reflections with intensity $I > 2\sigma$. Full-matrix least squares refinement on F^2 was performed on those 464 independent reflections and 62 parameters were refined. The final R ($I > 2\sigma$) indices are $R_1=0.089$ and $wR_2=0.0444$. Both the lattice parameters and atomic positions are in good agreement with those reported in Ref. 27. The lattice parameters are $a=9.177(2)$ Å, $b=12.152(2)$ Å, and $c=2.9891(5)$ Å, where the numbers in the parentheses give errors on the last digit. The occupation probabilities of vanadium atoms at VL1-VL4 sites are 0.82(1), 0.51(1), 0.40(1), and 0.56(1) respectively, which corresponds to a calculated $x=0.40(1)$.

Figure 2 shows the observed and calculated (from Rietveld refinement) powder x-ray diffraction patterns for a powder sample of $(Li_{0.33}V_{0.67})_3BO_5$. Bragg peak positions and the difference between the observed and calculated peak intensities are also displayed. Weak V_2O_3 impurity peaks are present in the pattern. The amount of V_2O_3 impurity is estimated from the two-phase Rietveld refinement to be ≈ 5 mol %. Isotropic thermal displacement parameters U were used during Rietveld refinement and their values were fixed to be equal to the equivalent thermal displacement parameter values U_{eff} for a single crystal obtained from the above single crystal refinement. The final agreement factors were $R_p=7.2\%$ and $R_{wp}=9.3\%$ and reduced $\chi^2=2.54$. The occupation probabilities of vanadium atoms at VL1–VL4 sites are 0.96(1), 0.52(1), 0.47(1), and 0.48(1), respectively, which corresponds to $x=0.35(1)$, in reasonable agreement with nominal value $x=0.33$. The lattice constants a, b, and c are 9.1820(2), 12.1540(3), and 2.9872(1) Å, respectively.

By applying Goodenough's rules, the sign and relative strength of magnetic interactions among neighboring vanadium moments can be inferred from the structure.[39] The vanadium atoms occupy octahedral interstices of the oxygen sublattice and the octahedra are connected by either edge or corner sharing. Table I lists the VL-VL nearest-neighbor distances and VL-O-VL bond angles. Since the vanadium cation has less than four d electrons in its outer shell, according to

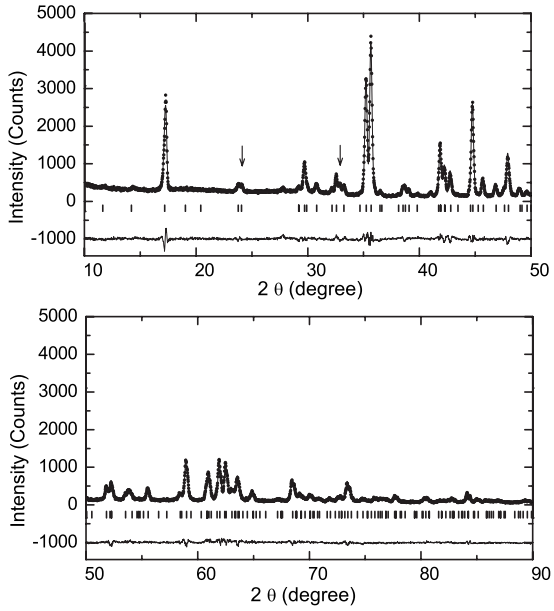

FIG. 2. Observed and calculated x-ray diffraction patterns for $(Li_{0.33}V_{0.67})_3BO_5$ powder. The upper trace shows the observed data by dots and the calculated pattern by the solid line. The lower trace is a plot of the difference between the observed and calculated intensities. The vertical bars show the positions for the Bragg reflections of $(Li_{0.33}V_{0.67})_3BO_5$. The observed diffraction pattern indicates the presence of ≈ 5 mol % of V_2O_3 phase as estimated from the two-phase Rietveld refinement of the data. The arrows indicate the positions of the two strongest V_2O_3 peaks.

Table I in Ref. 40, all nearest-neighbor vanadium-vanadium spin interactions are expected to be antiferromagnetic. For the edge sharing configuration, the vanadium-oxygen-vanadium interaction is expected to be much smaller than the direct vanadium-vanadium interaction which increases with decreasing distance.[40] Since the distance between nearest-neighbor VL1 and VL4 sites is much smaller than other VL-VL distances, Onoda[27] pointed out that the largest exchange interaction could exist between these two sites. Since each VL4 site is connected to two VL1 sites on either side, a VL1-VL4-VL1 linear spin trimer can be formed. In the next section, a detailed study of the linear trimer model will be

TABLE I. Distances and bond angles of nearest-neighbor VL-VL sites.

	Distance (Å)	VL-O-VL angle
	Corner sharing	
VL1-VL2	3.3725	119.6°
VL2-VL3	3.4366	119.8°
	Edge sharing	
VL1-VL2	3.0914	95.5° and 98.1°
VL1-VL3	2.9919	92.3° and 96.9°
VL1-VL4	2.7480	84.4° and 84.4°
VL2-VL4	3.0332	93.9° and 95.9°

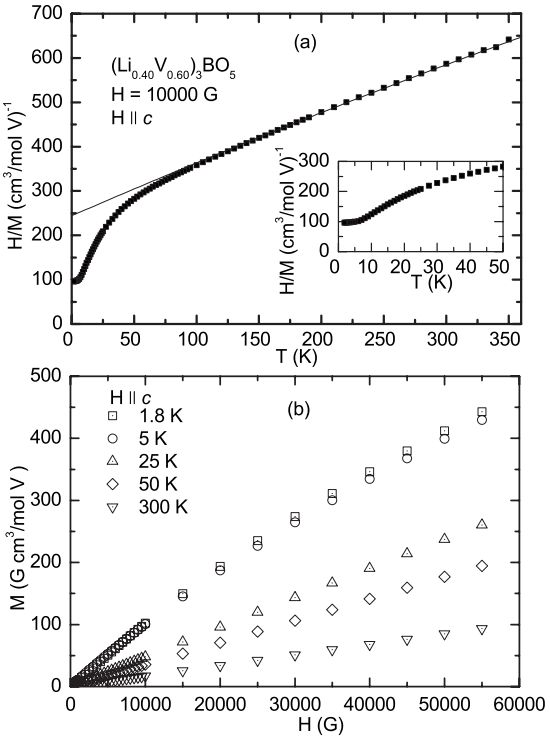

FIG. 3. Magnetization of the aligned $(Li_{0.40}V_{0.60})_3BO_5$ crystals with magnetic field $H \| c$. (a) Inverse magnetization over field, H/M, measured at $H=10\,000$ G. The data were taken during field cooling. The solid curve is a fit to the 200–350 K data by Eq. (1). Inset: Expanded plot of the low temperature data. (b) $M(H)$ isotherms at $T=1.8$, 5, 25, 50, and 300 K. A negative curvature was observed at 1.8 and 5 K.

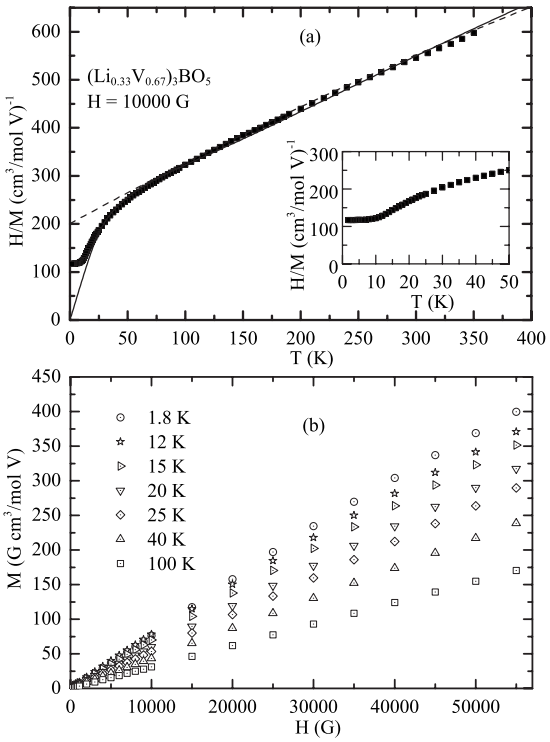

FIG. 4. Magnetization M of the $(Li_{0.33}V_{0.67})_3BO_5$ powder sample. (a) Inverse M over field H, H/M, versus T, measured at $H=10\,000$ G. The data were taken during field cooling. The dashed line is a fit to the 200–350 K data by Eq. (1) and the solid line is a fit to the 20–350 K data by Eq. (8). Inset: Expanded plot of the low temperature data. (b) M versus H isotherms at different temperatures.

presented in an attempt to explain the high temperature susceptibility results.

Given antiferromagnetic interactions among all nearest-neighbor vanadium spins, significant frustration for the magnetic interactions is expected. This is due to the presence of various triangles formed by nearest-neighbor VL sites, as one can see in Fig. 1. As a result, no spin configuration can minimize the exchange energy of all the vanadium-vanadium interactions. This geometric frustration effect is inherent in the structure and not induced by the disorder of the random Li and V occupation. The presence of both frustration and disorder is responsible for the low temperature spin-glass phase at $T \lesssim 10$ K.

IV. MAGNETIZATION

A. Magnetic susceptibility

Figures 3(a) and 4(a) display the inverse susceptibility $(M/H)^{-1}$ versus temperature T in the T range 1.8–350 K and at applied magnetic field $H=1$ T of the aligned crystals $(H \| c)$ and the powder sample, respectively. Both sets of data were taken during field cooling. Measurements done on crystals with the c axis parallel and perpendicular to the field gave almost the same results, indicating the absence of significant magnetic anisotropy in the system. As shown in Figs. 3(b) and 4(b), the magnetization M deviates from being proportional to H at low temperatures ($T \lesssim 20$ K for the powder sample). Such deviations are consistent with the appearance of a nonzero nonlinear susceptibility as the system approaches its spin-glass transition temperature.[41] The evidences for a spin-glass state at low temperatures ($T < 10$ K) will be discussed in detail below.

For both the single crystal sample and the powder sample, the high T ($T > 100$ K) region of the susceptibility can be described by a constant plus a Curie-Weiss term,

$$\chi(T) = \chi_0 + \frac{C}{T-\theta}. \tag{1}$$

A fit to the susceptibility data of the single crystals in the T range 200–350 K gives $\chi_0=0.0002(1)$ cm^3/mol V, $C=0.74(9)$ cm^3 K/mol V, and $\theta=-190(27)$ K. The constant term χ_0 arises mainly from the diamagnetism of the ion cores and the paramagnetic Van Vleck susceptibility of the vanadium atoms. We estimate χ^{core} to be -4.3×10^{-5} cm^3/mol V, using the values -0.6×10^{-6}, -10×10^{-6}, -7×10^{-6}, -35×10^{-6}, and -12×10^{-6} cm^3/mol for Li^+, V^{3+}, V^{4+}, $(BO_3)^{3-}$, and O^{2-} ions.[42] The Van Vleck susceptibility is thus $\chi^{\text{VV}}=\chi_0-\chi^{\text{core}}=0.0002(1)$ cm^3/mol V. This value is of the same order as the values of Van Vleck susceptibility of vanadium ions in LiV_2O_4, VO_2, and

TABLE II. Eigenstates, eigenvalues E, and degeneracies n of the linear trimer Hamiltonian [Eq. (3)].

E (J)	2	1	0	−1	−1	−2	−3
S_T	3	2	1	1	2	0	1
S_{13}	2	1	0	1	2	1	2
n	7	5	3	3	5	1	3

$LaVO_3$.[36] The value of the Curie constant C can be compared with that predicted by the molecular field theory.[43] Assuming that the vanadium atoms in the crystals are in either +3 (spin $S=1$) or +4 ($S=1/2$) oxidation states, the Curie constant is given by

$$C = \frac{N_A \mu_B^2}{3k_B}\left[2fg_1^2 + \frac{3}{4}(1-f)g_2^2\right], \tag{2}$$

where f is the fraction of trivalent vanadium moments and g_1 and g_2 are g factors for trivalent and tetravalent vanadium moments, respectively. $x=0.4$ corresponds to $f=0.8$. Equation (2) thus gives $C=0.82$ cm^3 K/mol V assuming $g_1=1.93$ (Ref. 44) and $g_2=1.97$,[45] respectively. This value is within the error bar of the observed Curie constant $C=0.74(9)$ cm^3 K/mol V.

A fit of Eq. (1) to the data of the powder sample in the T range 200–350 K gives $\chi_0=0.0003(1)$ cm^3/mol V, $C=0.67(5)$ cm^3 K/mol V, and $\theta=-143(16)$ K. In the polycrystalline sample, all the vanadium atoms are in the +3 charge state, so Eq. (2) gives $C=0.93$ cm^3 K/mol V assuming $f=1$ and $g=1.93$, which is much higher than the observed value. A second polycrystalline sample with the same composition $(Li_{0.33}V_{0.67})_3BO_5$ was made using the same procedure, and a fit of Eq. (1) to its susceptibility data in the same temperature range gave $C=0.56(6)$ cm^3 K/mol V, $\chi_0=0.0005(1)$ cm^3/mol V, and $\theta=-99(6)$ K. The Curie constants between the two powder samples match within experimental error, while there is a significant difference in the θ. The reason for the discrepancy in θ values is not known. We note that a lower than calculated Curie constant is also present in Ref. 27, where $C=0.77$ cm^3 K/mol V and $\theta=-125$ K for a powder sample with the same x value as our powder samples.

To understand the difference between the measured and expected Curie constants in the powder samples, we will first discuss the effect of V_2O_3 and possible amorphous $LiBO_2$ impurities on the magnetization results. The above Rietveld refinement of the powder x-ray diffraction data indicates that our powder sample contains 5 mol % V_2O_3 impurity. V_2O_3 undergoes a first order phase transition from paramagnetic metal to antiferromagnetic insulator at around 170 K. Above 170 K, it has an almost temperature-independent susceptibility[46] so this phase will not contribute to the high temperature Curie-Weiss term in Eq. (1). Its contribution to the constant term χ_0 is about 0.25×10^{-4} cm^3/mol V, which is within the error bar of the fitting result of χ_0. $LiBO_2$ is nonmagnetic and its contribution to the susceptibility should also be negligible. The presence of 5 mol % V_2O_3 impurities leads to an overestimation of the $(Li_{0.33}V_{0.67})_3BO_5$ sample mass by 5%, assuming that the same molar percentage of amorphous $LiBO_2$ impurity is present in the sample.

The above analysis shows that the presence of impurities is insufficient to explain our low observed Curie constants in the powder sample. The reason for this discrepancy is currently not understood. It is noted that molecular field theory predictions are generally valid only in the high temperature limit $T \gg |\theta|$, which is not satisfied in our temperature range 200–350 K due to the large values of $|\theta|$. However, this limitation should also apply to the single crystal case, where the discrepancy between observed and calculated Curie constants is much smaller, although the condition $T \gg |\theta|$ is even less satisfied due to the higher $|\theta|$ value in the crystals.

B. Linear trimer model

Below ~100 K, the slope of the H/M versus T curve increases with decreasing temperature. As proposed in Ref. 27, this could be due to the existence of spin trimers with antiferromagnetic nearest-neighbor interactions. A spin trimer has a low spin ground state, which is separated from the first excited state by an energy gap of the order of the exchange constant J. At temperatures $T \ll J$, the effective number of spins is reduced, which results in a reduction of the effective Curie constant. So, the slope at low temperature increases in Figs. 3(a) and 4(a) since it is inversely proportional to the Curie constant. The possibility of trimer formation was indicated by the short distances between VL1 and VL4 sites as discussed in Sec. III. The expected behavior of susceptibility versus temperature in this trimer model can be analyzed most easily when all the vanadium spins have the same spin value. This is the case in the polycrystalline sample where all vanadium spins have $S=1$.

The Hamiltonian for a linear trimer can be written as

$$\mathcal{H} = J(\mathbf{S}_1 \cdot \mathbf{S}_2 + \mathbf{S}_2 \cdot \mathbf{S}_3) = \frac{J}{2}[(\mathbf{S}_1 + \mathbf{S}_2 + \mathbf{S}_3)^2 - (\mathbf{S}_1 + \mathbf{S}_3)^2 - \mathbf{S}_2^2]$$

$$= \frac{J}{2}[\mathbf{S}_T^2 - \mathbf{S}_{13}^2 - 2], \tag{3}$$

where $J>0$ is the antiferromagnetic nearest-neighbor exchange coupling constant between vanadium moments at adjacent VL1 and VL4 sites, $\mathbf{S}_1$ and $\mathbf{S}_3$ are the spins at the two VL1 sites at the two ends of a trimer, $\mathbf{S}_2$ is the spin at the VL4 site in the middle of the trimer, and $\mathbf{S}_T \equiv \mathbf{S}_1+\mathbf{S}_2+\mathbf{S}_3$ and $\mathbf{S}_{13} \equiv \mathbf{S}_1+\mathbf{S}_3$. The different eigenstates of this Hamiltonian as well as their corresponding energy eigenvalues and degeneracies are listed in Table II. The partition function Z_T and molar spin susceptibility χ_T of the trimers are

$$Z_T = \sum_i n_i e^{-E_i/k_B T} \tag{4}$$

and

$$\chi_T = \frac{N_A g^2 \mu_B^2}{3k_B T Z_T} \sum_i n_i S_{Ti}(S_{Ti}+1) e^{-E_i/k_B T}, \tag{5}$$

where the index i runs over all the different states listed in Table II.

One also needs to consider the presence of dimers. Dimers are formed when one of the VL1 sites at the two ends of the trimer is instead occupied by a Li atom. The molar spin susceptibility of dimers consisting of two spins 1 can be obtained in the same way and the result is

$$\chi_D = \frac{N_A g^2 \mu_B^2}{k_B T Z_D}(10e^{-3J/k_B T} + 2e^{-J/k_B T}), \tag{6}$$

where $Z_D = 5e^{-3J/k_B T} + 3e^{-J/k_B T} + 1$ is the partition function of the dimer Hamiltonian. At temperatures much higher than the typical interactions between the dimer, trimer, and isolated spins, which is presumably of the order of the zero-field spin-glass transition temperature $T_g \lesssim 10$ K,[43] the total susceptibility of the system is

$$\chi = \frac{f_3}{3}\chi_T + \frac{f_2}{2}\chi_D + \frac{2N_A g^2 \mu_B^2}{3k_B T}(1 - f_2 - f_3) + \chi_0, \tag{7}$$

where f_2 and f_3 are the fractions of vanadium atoms belonging to dimers and trimers, respectively, and the third term gives the contribution from isolated $S=1$ spins. Equation (7) with $g \approx 2$ does not fit the experimental data over any appreciable temperature range with f_2, f_3, J, and χ_0 as free fitting parameters. However, a reasonable fit to the data can be achieved after scaling the temperature-dependent part by a prefactor $b < 1$:

$$\chi = b\left[\frac{f_3}{3}\chi_T + \frac{f_2}{2}\chi_D + \frac{2N_A g^2 \mu_B^2}{3k_B T}(1 - f_2 - f_3)\right] + \chi_0. \tag{8}$$

The prefactor $b < 1$ is introduced as an attempt to isolate the unknown effects causing the difference between calculated and measured Curie constants discussed in Sec. IV A. Shown as the solid curve in Fig. 4 is the fitting result of Eq. (8). The best-fit parameters are $f_2 = 0.76(18)$, $f_3 = 0.04(29)$, $J = 109(17)$ K, and $b = 0.61(1)$ with χ_0 fixed to 0.0003 cm^3/mol V and g fixed to 1.93. From the occupation probabilities of vanadium atoms at VL1–VL4 sites as determined from Rietveld refinement, one expects

$$f_2 = \frac{4p_1 p_4(1-p_1)}{2p_1 + 2p_2 + p_3 + p_4} = 0.02 \tag{9}$$

and

$$f_3 = \frac{3p_1^2 p_4}{2p_1 + 2p_2 + p_3 + p_4} = 0.34, \tag{10}$$

where p_1–p_4 are the occupation probabilities of vanadium atoms at the VL1–VL4 sites, respectively. The expected values are in large discrepancy with the above fitting results of $f_2 = 0.76$ and $f_3 = 0.04$. We conclude that the above model of isolated monomers, dimers, and trimers cannot explain the susceptibility data at high temperatures. Most likely, interactions between those spin objects need to be considered and antiferromagnetic spin clusters form as the temperature approaches the zero-field T_g from above, which results in a reduction of the effective Curie constant and a negative curvature in inverse susceptibility versus temperature, qualitatively similar to the behavior expected from the above spin trimer model.

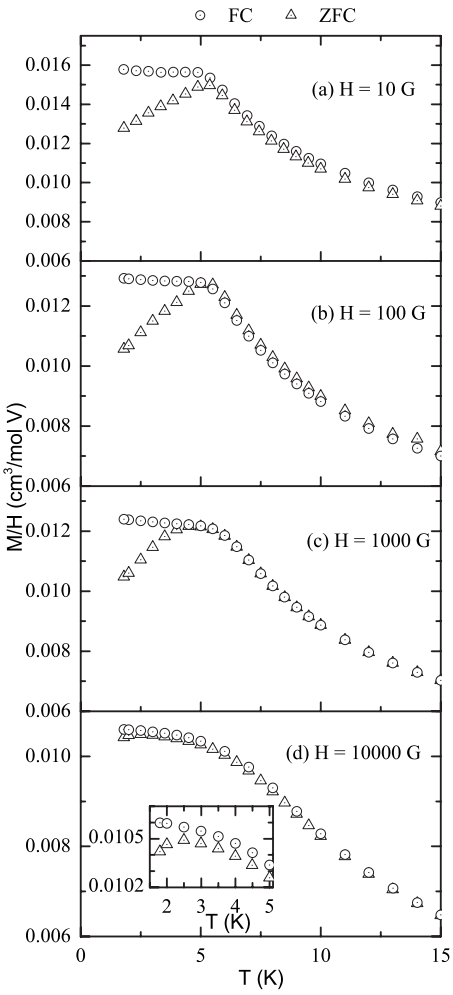

FIG. 5. Splitting of field-cooled (FC) and zero-field-cooled (ZFC) magnetization M versus temperature T of $(Li_{0.40}V_{0.60})_3BO_5$ crystals at low temperatures and $H = 10$, 100, 1000, and 10 000 G. The FC magnetizations were measured on cooling. The inset on the bottom panel is an expanded plot of the low temperature region.

C. Spin-glass behavior

In order to confirm the spin-glass state at low temperatures as proposed in Ref. 27, we first compare the magnetization results measured at zero-field-cooled (ZFC) and field-cooled (FC) conditions. Figure 5 shows the splitting of ZFC and FC magnetization at low temperatures at $H = 10$, 100, 1000, and 10 000 G in the aligned single crystals. The FC magnetization was measured on cooling. For the polycrystalline sample, a similar splitting is observed below 8.5 K at

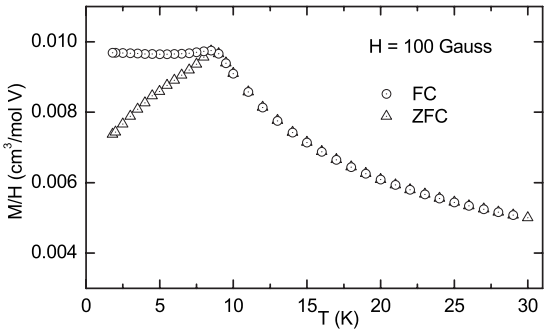

FIG. 6. Splitting of field-cooled (FC) and zero-field-cooled (ZFC) magnetization M versus temperature T of the $(Li_{0.33}V_{0.67})_3BO_5$ powder sample below $T_g=8.5$ K and at $H=100$ G. The FC magnetization was measured on cooling.

$H=100$ G, as shown in Fig. 6. The ZFC-FC bifurcation is a signature for the presence of a spin-glass state at low temperatures. The onset temperature of ZFC and FC magnetization splitting at the lowest field is referred to as the zero-field spin-glass transition temperature T_g throughout the paper. For the single crystals $T_g=5.5$ K, while for the powder sample $T_g=8.5$ K. The ratio $|\theta|/T_g$ is an empirical measure of geometric frustration in a system.[47] This ratio is 35(5) and 17(2) for our crystal and polycrystalline samples, respectively, indicating the presence of strong frustration in the system. It is noted in Fig. 5 that even above T_g, there are slight differences between zero-field-cooled and field-cooled magnetizations. However, these slight differences are within the experimental error and are not related to the spin-glass behavior. The magnitude of ZFC-FC bifurcation was gradually suppressed and the onset temperature of the strong bifurcation decreases with increasing magnetic field. This suggests that the spin-glass transition temperature is suppressed to lower temperatures with increasing field. In the next section, we will apply NMR to further study the effect of magnetic fields on the spin dynamics of the system.

In a ferromagnetic sample, similar ZFC-FC splitting could arise due to the presence of domain walls between neighboring ferromagnetic domains.[48] In order to exclude such a possibility, we performed measurements of hysteresis loops. Figure 7(a) displays the magnetization M versus applied magnetic field H in the aligned crystals as the field was cycled between −5.5 and 5.5 T at $T=1.8$ and 4.2 K. The curves were taken immediately after the crystal was zero-field cooled to 1.8 or 4.0 K from above 5.5 K. The hysteresis of the M versus H curves observed with field cycling is very small, as shown in the inset of Fig. 7(a). The absence of significant hysteresis suggests that a ferromagnetic transition is not the origin of the ZFC-FC splitting.

Slow decaying of thermal remnant magnetization is considered as one of the defining properties of spin-glass systems.[49] Figure 7(b) shows the decrease with time of the remnant magnetization after turning off a field $H=1000$ G at 2.0 K. The field was turned off immediately after the crystals were field cooled to 2.0 K from above 5.5 K. The long time behavior can be fitted by a stretched exponential function,

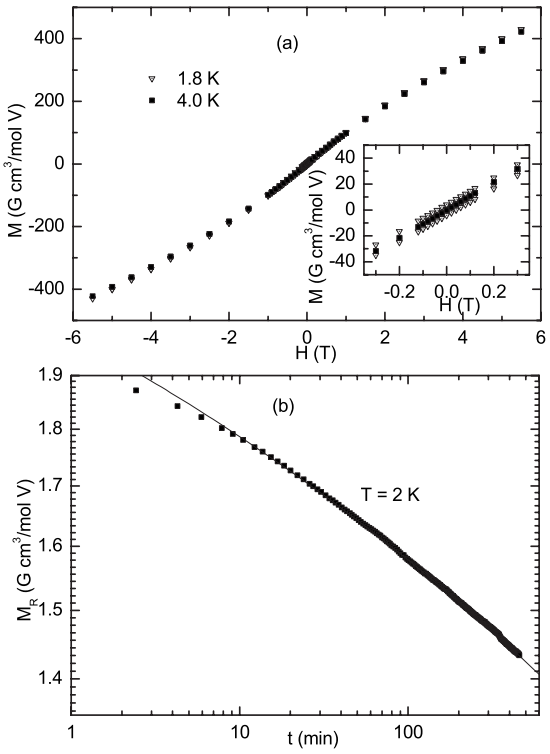

FIG. 7. (a) Magnetization M versus the external magnetic field H in the aligned single crystals as H was cycled between 5.5 and −5.5 T at $T=4.2$ and 1.8 K. The field was parallel to the c axis. Inset: Expanded plot of the low field region. (b) Relaxation of remnant magnetization M_R of crystals versus time t after turning off a field of 1000 G at 2.0 K immediately after field cooling from above 5.5 K. The solid curve is a fit by Eq. (11) to the data at $t>18$ min.

$$M_R(t) = M_0 \exp[-(t/\tau)^{\beta}]. \tag{11}$$

The best fit to the data at $t>18$ min (solid line in Fig. 7) gave $M_0=3.24(6)$ G cm^3/mol V, $\tau=7300(1400)$ min, and $\beta=0.086(2)$. Relaxation as described by Eq. (11) with similar values of β was observed in other spin-glass systems.[50,51]

To further confirm the spin-glass state of the system, we studied memory and rejuvenation effects in $(Li_xV_{1-x})_3BO_5$, following the method used by Sun *et al.*[52] The main panel of Fig. 8 shows the development of magnetization following application of a 50 G magnetic field immediately after the crystal was zero-field cooled to 3.0 K from above 5.5 K. The crystal was then quickly cooled to 1.8 K after staying at 3.0 K for $t_1\approx260$ min. A sharp increase of magnetization was observed right after the cooling. However, after the temperature was increased back to 3.0 K after another $t_2\approx230$ min, the magnetization returned back to the value just before cooling to 1.8 K and the magnetization continued to evolve as if the t_2 stage did not take place. Such a memory effect was not observed if the temperature during the t_2 stage was higher than during t_1 and t_3. As displayed in the inset of Fig. 8, where the respective temperatures during t_2 and during t_1 and t_3 were switched, the magnetization at the beginning of t_3 did not return to the value right before the temperature change to 3.0 K took place. Instead, the

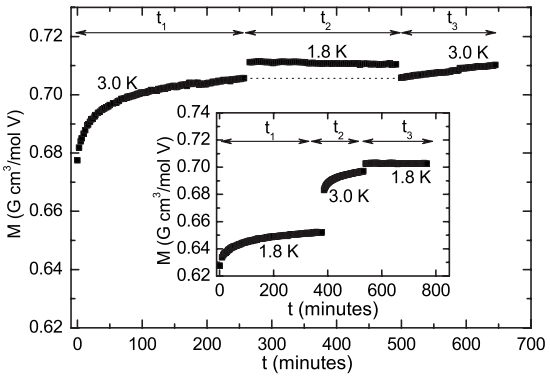

FIG. 8. Memory and rejuvenation effects in the aligned single crystals of $(Li_{0.4}V_{0.6})_3BO_5$. The field was parallel to the c axis. Main panel (inset): Development of magnetization after turning on a field of 50 G immediately after the crystals were zero-field cooled to 3.0 K (1.8 K). After time t_1, the temperature was quickly changed to 1.8 K (3.0 K) and kept at that temperature for time t_2. Then, the temperature was changed back to 3.0 K (1.8 K). The field was kept at 50 G during the whole process.

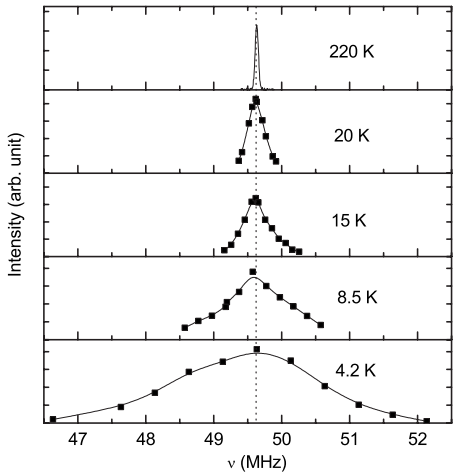

FIG. 9. ^{7}Li NMR spectrum at temperatures T=220, 20, 15, 8.5, and 4.2 K and an external magnetic field H=3 T. The spectrum at 220 K was obtained by Fourier transform of half echo signal, while spectra at low temperatures were obtained by frequency sweep. The squares are data points and the solid lines are guides for the eye. The zero-field spin-glass transition temperature is T_g=8.5 K (see text). The vertical dotted line marks the position of the ^{7}Li resonance in aqueous lithium chloride solution.

rejuvenation effect was observed right after the temperature changed to 3.0 K (at the beginning of stage t_2): the magnetization reinitialized as if the t_1 stage did not take place. The asymmetry effects between heating and cooling during t_2 could be attributed to a hierarchical organization of the free energy landscape in the spin-glass phase space.[52,53] It is noted that recent studies demonstrate that the above memory and rejuvenation effects can also arise from a collection of isolated nanoparticles with a temperature-dependent distribution of relaxation times.[54] However, considering the random distribution of Li and V atoms within the structure, the occurrence of isolated nanoclusters should have a very small probability.

V. NMR

A. Introduction

We carried out nuclear magnetic resonance (NMR) studies in order to further study the spin freezing properties in strong magnetic field of a material that has a spin-glass transition in zero field. Furthermore, we investigated the dynamical inhomogeneities in the system and extracted the distribution of electronic spin relaxation times from nuclear spin-lattice relaxation measurements.

A search for a ^{51}V NMR signal was performed in the frequency range 51.8–53.1 MHz at T=295 K and H=4.7 T (Larmor frequency=52.6 MHz). The separation between the two rf pulses which could generate an echo was 20 μs. Considering the possibility of a strong quadrupole effect which could decrease the $\pi/2$ pulse length of the central transition,[55] various pulse length combinations were used at each frequency. However, no ^{51}V NMR signal could be detected under the above conditions. We thus performed NMR measurements on ^{7}Li and ^{11}B nuclei as follows. Both ^{7}Li and ^{11}B nuclei have spin I=3/2. No observable quadrupole effect was observed for ^{7}Li, while ^{11}B displayed clear quadrupole splitting in the spectrum. The difference is attributed to different local electric field gradients (EFGs) of these two nuclei, since the quadrupole moment of ^{7}Li nucleus is 2.8 times that of ^{11}B.[56] All NMR measurements were performed on the powder sample of $(Li_{0.33}V_{0.67})_3BO_5$ which has a zero-field spin-glass temperature of 8.5 K, as shown previously in Fig. 6.

B. ^{7}Li NMR spectrum

The ^{7}Li NMR spectrum in the powder $(Li_{0.33}V_{0.67})_3BO_5$ sample shows a single line without an observable quadrupolar effect. A strong broadening of the spectrum is observed with decreasing temperature. Figure 9 displays the spectrum at H=3 T at different temperatures. In contrast to the strong inhomogeneous broadening, the peak positions of the spectra remain almost temperature independent (shift $<$0.1% of the resonant frequency), consistent with broadening due to dipolar interactions with vanadium local moments with weak g-factor anisotropy.[57,58]

The temperature dependence of the full width at half maximum (FWHM) peak intensity of the spectra is plotted in Fig. 10. The FWHM versus T at $T>8.5$ K can be well fitted by a Curie-Weiss law plus a constant,

$$\mathrm{FWHM} = C_0 + C_1/(T-\theta_1), \tag{12}$$

where the best-fit parameters are C_0=38(3) kHz, C_1=3.5(4) MHz, and θ_1=5.5(7) K. This fit is plotted as the solid line in Fig. 10. The following analysis shows that the strong broadening of the spectrum at low temperatures must be due to inhomogeneity of static local magnetic fields (inhomogeneous broadening). The intrinsic linewidth of each ^{7}Li nuclear spin is of the order of $1/T_2$, the inverse of spin-

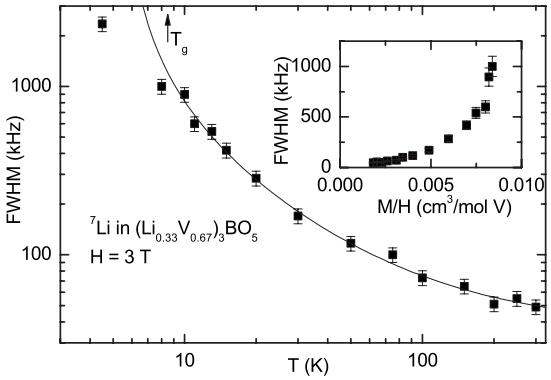

FIG. 10. Full width at half maximum (FWHM) peak intensity of the ^{7}Li NMR spectrum versus temperature T at applied magnetic field $H=3.00$ T. The vertical arrow indicates the zero-field spin-glass transition temperature $T_g=8.5$ K. The solid curve is a phenomenological fit by Eq. (12). Parameters for the fit are given in the text. Inset: FWHM varsus magnetization divided by field M/H at $H=3.00$ T with temperature as the implicit variable.

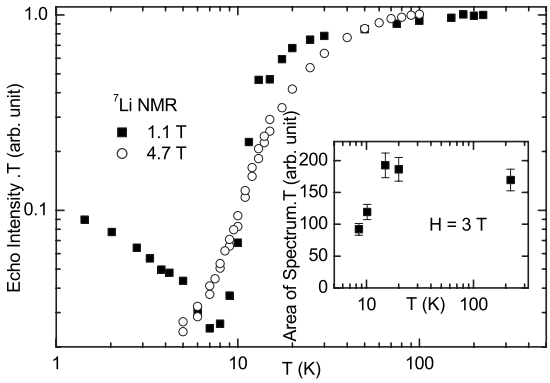

FIG. 11. Temperature T dependence of normalized ^{7}Li NMR echo intensity at $H=1.1$ and 4.7 T. Inset: T times area of the whole spectrum at $H=3.0$ T after correction for the T_2 effect.

spin relaxation time. As will be shown below in Table III, the effective spin-spin relaxation time for the detected ^{7}Li nuclear spins is $\gtrsim 100$ μs at $T>8.5$ K, which corresponds to an intrinsic linewidth of the order of 10 kHz, much smaller than the observed linewidth below ~ 50 K (see Fig. 10). The full width at half maximum at 4.2 K is approximately 2 MHz, corresponding to a local field distribution of width ~ 0.1 T. This width is of the same order as the root mean square values of the local dipolar fields at the ^{7}Li nuclear sites, as will be shown below [see Eqs. (17) and (20)].

The inset of Fig. 10 shows FWHM versus M/H at $H=3.00$ T with temperature as the implicit variable. At $T \lesssim 30$ K, FWHM deviates strongly from being proportional to magnetization and increases much faster than the magnetization with decreasing temperature. One possible explanation of such deviation might be the occurrence of antiferromagnetically coupled clusters. In systems with dense paramagnetic moments, the inhomogeneous broadening is proportional to $\sqrt{n}\langle S_z\rangle$, where n and $\langle S_z\rangle$ are the concentration and field-induced spin polarizations of the paramagnetic moments, respectively.[56] On the other hand, the magnetization M is proportional to $n\langle S_z\rangle$. The concentration n of *effective* paramagnetic moments decreases in the system if small antiferromagnetic clusters (including the above mentioned spin dimers and trimers in their ground states) occur with decreasing temperature. Because of the above different dependences of FWHM and M on concentration n, the FWHM increases faster than M with decreasing temperature. We note that the formation of antiferromagnetic spin clusters is qualitatively consistent with the negative curvature in inverse susceptibility versus temperature below $T\sim 100$ K in Figs. 3(a) and 4(a) as discussed in Sec. IV B above.

C. ^{7}Li NMR signal intensity

A minimum in normalized NMR signal intensity was observed long ago in metallic spin glass systems close to the zero-field spin-glass transition temperature.[29,32] The normalized echo intensity for ^{7}Li in $(Li_{0.33}V_{0.67})_3BO_5$ at $H=1.1$ and 4.7 T shows similar behavior, as displayed in the main panel of Fig. 11. The echo intensity was measured by the area under the absorption line obtained through Fourier transformation of half the echo signal and was normalized by multiplying by T to compensate for the nuclear Curie law for the equilibrium longitudinal nuclear magnetization. The resulting value should then be proportional to the number of ^{7}Li nuclei detected in the experiments. Two factors can contribute to the loss of this signal intensity. The first factor is the limited frequency window of the NMR spectrometer ($\Delta f \sim 200$ kHz). Due to the strong inhomogeneous broadening of the spectrum at low temperatures, the nuclei with a resonant frequency outside the NMR spectrometer window cannot be detected. The second factor is the shortening of the spin-spin relaxation times around the spin-glass transition temperature. Since the $\pi/2$ and π pulse separation for echo generation was fixed to 20 μs, a reduction of T_2 to less than 40 μs can also result in a decrease of signal intensity.

These two factors can be partly compensated by measuring the area of the whole absorption spectrum and then multiplying by a T_2 correction factor.[59] To carry out the compensation, we first integrate the spectra in Fig. 9, with the spectra further away from the measured parts estimated by linearly extrapolating the wings until zero intensity was reached. In order to determine the T_2 correction factor at

TABLE III. ^{7}Li nuclear spin-spin relaxation times at $H=3.0$ T and different temperatures. The parameters T_2 and T_{2g} are defined in Eq. (13).

T (K)	8.5	10.2	15	20	90	175	295
T_2 (μs)	76(4)	88(5)	258(13)	442(22)	∞	∞	∞
T_{2g} (μs)	∞	∞	712(35)	571(29)	359(18)	293(15)	307(15)

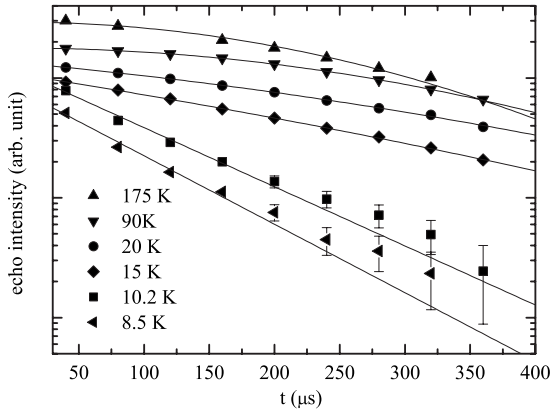

FIG. 12. ^{7}Li NMR echo intensity versus twice the pulse spacing t between the $\pi/2$ and π pulses that generate an echo at different temperatures at $H=3.0$ T. The solid lines are fits by Eq. (13) with parameter values listed in Table III.

each temperature, spin-spin relaxation rates were measured at a few temperatures, as shown in Fig. 12. At high temperatures, the ^{7}Li nuclear magnetization versus rf pulse separation follows square exponential decay (half Gaussian), while it crosses over to a single exponential decay with decreasing temperatures. We describe the decay of the spin-echo amplitude by the expression

$$A(t) = A_0 \exp[-(t/T_{2g})^2 - t/T_2]. \quad (13)$$

Table III lists the values of T_{2g} and T_2 at different temperatures. It was found that the values of T_{2g} and T_2 at different parts of the spectrum are almost the same and so a single T_2 correction factor is used for the whole spectrum. The inset of Fig. 11 shows the T dependence of T times the area of the whole spectrum after multiplying by the T_2 correction factor $\exp[(t/T_{2g})^2 + t/T_2]$ with $t=40$ μs. The signal loss at high temperatures is now fully recovered. However, at $T \lesssim 15$ K, close to the zero-field spin-glass transition temperature, signal intensity loss is still observed. This indicates that at $T \lesssim 15$ K, some of the nuclei have T_2 values much shorter than 40 μs and so their signal cannot be compensated by the above T_2 correction factor, rendering them unobservable [see Fig. 15 and the discussion following Eq. (19) below].

D. ^{7}Li nuclear spin-lattice relaxation

The recovery of the longitudinal nuclear magnetization $M(t)$ following saturation changes from a single exponential to a stretched exponential function as the system approaches the zero-field spin-glass transition temperature T_g from above, as displayed in Fig. 13. Due to the strong inhomogeneous broadening of the spectrum, it became difficult to saturate the whole line with the rf comb pulses and only the central part of the spectrum can be saturated. A possible origin for the observed stretched exponential is thus spectral diffusion, i.e., transfer of Zeeman energy from saturated to unsaturated spins at other parts of the spectrum. In order to check such a possibility, the nuclear spin-lattice relaxation measurements at 4.7 T and below 15 K were performed us-

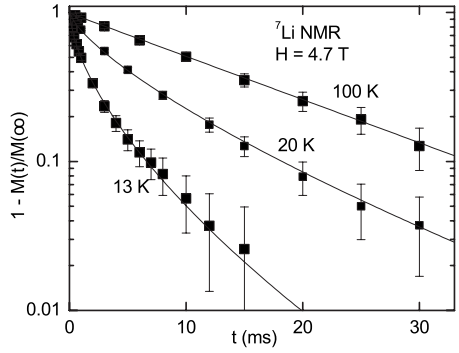

FIG. 13. ^{7}Li NMR nuclear spin-lattice relaxation curves in $(Li_{0.33}V_{0.67})_3BO_5$ powder sample following a saturation pulse sequence at $H=4.7$ T and $T=100$, 20, and 13 K. Solid curves are fits by Eq. (14).

ing two different saturation pulse sequences. The first saturation sequence consisted of 20 $\pi/2$ pulses with separation between neighboring pulses equal to 50 μs, while the second saturation sequence consisted of 10 $\pi/2$ pulses with separation between neighboring pulses of 300 μs. The duration of the $\pi/2$ pulses is equal to 4.7 μs in both cases. The recovery curves obtained in both conditions were the same at each temperature, which strongly suggests that the observed nonexponential recovery is intrinsic to the sample and is not related to artificial effects such as spectral diffusion. The effect of spectral diffusion depends on the degrees of saturation of the nuclear spins away from the center of the spectrum, which are expected to be different between the above two pulse sequences.

$M(t)$ can be fitted with a stretched exponential function with a variable $1/T_1^*$ and variable exponent β,

$$1 - \frac{M(t)}{M(\infty)} = \exp[-(t/T_1^*)^\beta]. \quad (14)$$

The physical meanings of the parameters $1/T_1^*$ and β have been discussed in recent papers.[33,35] Figure 14 shows the temperature dependence of $1/T_1^*$ and β at $H=1.1$ and 4.7 T.

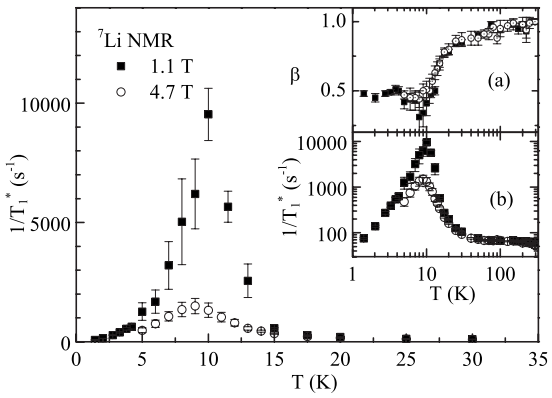

FIG. 14. ^{7}Li nuclear spin-lattice relaxation rates $1/T_1^*$ in Eq. (14) versus temperature T at $H=1.1$ and 4.7 T. Inset (a): Exponent β versus T. Inset (b): Log-log plot of $1/T_1^*$ versus T.

Note that the results at low temperatures ($T<20$ K) were obtained from measurements on only a small fraction of ^{7}Li nuclei in the system (see Fig. 11). The crossover from a single exponential to stretched exponential relaxation is represented by β decreasing below unity with decreasing T. $1/T_1^*(T)$ shows a sharp enhancement close to the zero-field spin-glass transition temperature T_g in both fields. While $1/T_1^*$ strongly depends on the field close to the transition temperature, $\beta(T)$ is almost temperature and field independent near and below T_g.

In the limit of small perturbation of nuclear Zeeman levels as is usual in NMR, one can apply the weak collision formula for the nuclear spin-lattice relaxation rate (NSLR), where NSLR arises from the Fourier component at $\omega_n=\gamma H$ of the fluctuating magnetic field arising from the fluctuating electronic spins:[60]

$$\frac{1}{T_1}=\frac{\gamma_{\mathrm{Li}}^2}{2}\int_{-\infty}^{\infty}\langle h_x(0)h_x(t)+h_y(0)h_y(t)\rangle\exp(-i\omega_n t)dt$$

$$=\frac{1}{2}\gamma_{\mathrm{Li}}^2\langle h_x^2+h_y^2\rangle\int_{-\infty}^{\infty}f(t)\exp(-i\omega t)\,dt\big|_{\omega=\omega_n}$$

$$\equiv\frac{1}{2}\gamma_{\mathrm{Li}}^2\langle h_x^2+h_y^2\rangle J(\omega)\big|_{\omega=\omega_n}, \tag{15}$$

where $\omega_n=\gamma_{\mathrm{Li}}H$ is the nuclear Larmor angular frequency, $\langle\cdots\rangle$ denotes a thermal average,

$$f(t)\equiv\frac{\langle h_x(0)h_x(t)\rangle}{\langle h_x^2\rangle}=\frac{\langle h_y(0)h_y(t)\rangle}{\langle h_y^2\rangle}$$

is the reduced correlation function of the local fluctuation field, and $J(\omega)$ is the Fourier transform of $f(t)$. We assume the correlation function $f(t)$ to be isotropic in the x-y plane which is perpendicular to the external field.

As noted in the Introduction, the occurrence of a stretched exponential relaxation may indicate the presence of a distribution of $1/T_1$ values. The distribution can arise from an inhomogeneity in the local fluctuating field $\langle h_x^2+h_y^2\rangle$ and/or an inhomogeneity in the dynamics seen by different nuclear spins. As discussed in the Introduction, whether or not dynamical inhomogeneity exists in spin glasses is still an unsettled issue. However, based on the following two considerations, we believe that the dynamical inhomogeneity is relevant in explaining our NMR results. First, the concentration of vanadium moments in the present system is very high and most ^{7}Li nuclei are expected to have a few nearest-neighbor vanadium moments that dominate their relaxation. As a result, the distribution of the local field is relatively narrow. Second, the value of β decreases continuously with decreasing temperature, which indicates an evolving $1/T_1$ distribution.[33,35] Similar conclusions were previously reached on the same basis from muon spin depolarization measurements on metallic spin glasses.[21] This is consistent with a temperature-dependent distribution of electronic spin relaxation times close to and above the spin-glass transition temperature derived from earlier experiments.[16,19,20]

Under conditions discussed below, the distribution of electronic spin relaxation times can be derived from the $1/T_1$ distribution of the ^{7}Li spins. Numerical studies suggested that an individual electronic spin autocorrelation function is not a pure exponential.[22,24] However, in order to make progress, we assume an electronic spin autocorrelation function $f(t)=e^{-|t|/\tau}$ as seen by a particular ^{7}Li nucleus, and then the nuclear spin-lattice relaxation rate of that ^{7}Li nucleus is

$$\frac{1}{T_1}=\gamma_{\mathrm{Li}}^2\langle h_x^2+h_y^2\rangle\frac{\tau}{1+\omega_n^2\tau^2}. \tag{16}$$

In order to calculate the value of τ from $1/T_1$, the value for $\langle h_x^2+h_y^2\rangle$ has to be determined. To compute this value, we will use the spatial average $\overline{\langle h_x^2+h_y^2\rangle}$ over all the ^{7}Li nuclear positions and estimate the average with the following simplifying assumptions. First, we assume an isotropic superexchange interaction among neighboring vanadium spins. In such a case, the fluctuation of the transverse components of a spin will be modulated by an oscillation with the electronic Larmor frequency and its spectral density at the frequency of the nuclear Larmor frequency is very small.[61] Thus, one only needs to consider the local field fluctuation due to the longitudinal components of vanadium spins. Second, we ignore possible correlations between the fluctuations of local fields produced by different vanadium local moments. Then,[56]

$$\langle h_x^2+h_y^2\rangle=\sum_i\frac{3\gamma_s^2\hbar^2}{r_i^6}(\sin^2\theta_i\cos^2\theta_i)S(S+1), \tag{17}$$

where $\hbar$ is Planck's constant divided by 2π, γ_s and S are respectively the gyromagnetic ratio and spin $S=1$ of the vanadium moments, r_i is the distance between vanadium moment i and the nuclear spin, and θ_i is the angle between $\vec{r}_i$ and the external field. In the numerical calculation, the applied magnetic field direction is arbitrarily chosen to be along the c axis. The four VL sites are randomly assigned with either Li or V atoms with the probability for vanadium atoms to be at VL1–VL4 sites of 0.913, 0.535, 0.460, and 0.501, respectively, as determined from Rietveld refinement. Our numerical calculations then give $(\overline{\langle h_x^2+h_y^2\rangle})^{1/2}=0.15$ T.

Now, the distribution of electronic spin relaxation times τ can be calculated by using an algorithm similar to that recently discussed in Ref. 35 in order to extract the distribution of relaxation rate values from a given stretched exponential recovery. In fact, from a given value of β in the stretched exponential function, one obtains a unique probability distribution $q(s,\beta)$ of $s=T_1^*/T_1$.[33,35] According to Eq. (16), for $\omega_n\tau<1$ (i.e., in the high temperature region above the zero-field T_g), a given value of $1/T_1$ corresponds to a unique value of τ where we use the above $\overline{\langle h_x^2+h_y^2\rangle}=0.0225$ T^2. The distribution of τ values can be expressed in the limit of $\omega_n\tau\ll1$ (justified *post hoc* in Fig. 15) by

$$p(\tau)=\frac{\tau}{a}q\left(\frac{\tau}{a},\beta\right), \tag{18}$$

where $p(\tau)d\tau/\tau=p(\tau)d\ln\tau$ is the probability that the relaxation time is between τ and $\tau+d\tau$ and is normalized according to $\int_{-\infty}^{\infty}p(\tau)d\ln\tau=1$, $q(s,\beta)$ is normalized according to $\int_0^{\infty}q(s,\beta)ds=1$, and

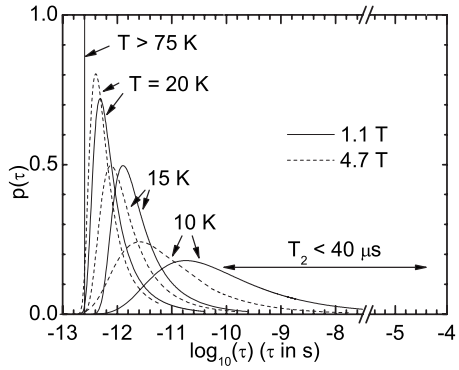

FIG. 15. Plots of the distribution of electronic correlation times τ extracted from ^{7}Li nuclear spin-lattice relaxation measurements at different temperatures and at fields $H=1.1$ and 4.7 T. At $H=1.1$ T, the β values are equal to 1, 0.78, 0.7, and 0.41 at temperatures $T>75$ K and $T=20$, 15, and 10 K, respectively. At $H=4.7$ T, the β values are equal to 1, 0.8, 0.7, and 0.5 at temperatures $T>75$ K and $T=20$, 15, and 10 K, respectively. The range indicated by the double arrowed line corresponds to values of τ which give rise to $T_2<40$ μs, for which the ^{7}Li NMR signal is not observable.

$$a = \frac{1}{\gamma_{\mathrm{Li}}^2 \overline{\langle h_x^2 + h_y^2 \rangle} T_1^*}.$$

The determination of the distribution $p(\tau)$ is an important result of the NMR measurements. $p(\tau)$ is plotted in Fig. 15 at a few temperatures and at fields $H=1.1$ and 4.7 T, where the β values at different temperatures are indicated in the figure caption. Because the fraction of ^{7}Li nuclei from which the $p(\tau)$ is determined becomes small as the temperature decreases below 15 K (see Fig. 11), the results should only be taken as an order of magnitude estimate. However, the trend of a slowing down and continuous broadening of the distribution is clearly seen as the zero-field spin-glass transition temperature is approached from above. Such a temperature dependence is qualitatively similar to distributions derived earlier from ac susceptibility and neutron spin-echo measurements.[16,19,20] One can see that even at 10 K, there still exist a significant amount of spins with very short correlation times: $\tau \sim 10^{-11}$ s. Such short τ values are in contradiction with the assumption $\gamma H \gg \frac{1}{\tau_{\min}}$ made in Ref. 25, from which the authors ruled out the dynamic inhomogeneity as an adequate description of the nonexponential spin-correlation function. Furthermore, one finds that at higher magnetic field, the overall relaxation rate tends to increase.

It is noted that the signal intensity loss (inset of Fig. 11) is consistent with the behavior of $p(\tau)$ in Fig. 15. In fact, the range indicated by the double arrowed line corresponds to values of τ with $T_2 \leqslant 40$ μs. An NMR signal from nuclear spins with such short T_2 values cannot be detected because the pulse separation between the two pulses which generate an echo signal is 20 μs. The value of τ above which the NMR signal becomes unobservable is $\tau=9.0\times10^{-11}$ s as estimated from the equation[62] (by setting $T_2=40$ μs)

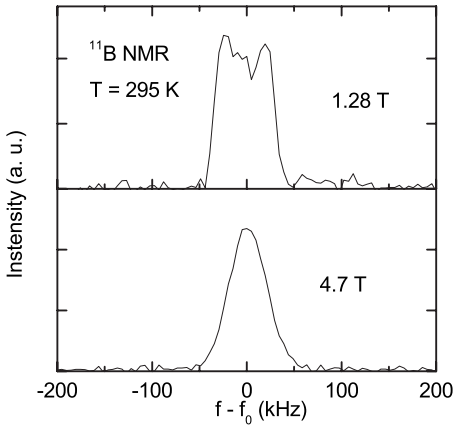

FIG. 16. Spectra of ^{11}B NMR central transition at $H=1.28$ and 4.7 T and $T=295$ K.

$$\frac{1}{T_2} = \frac{1}{2T_1} + \gamma_{\mathrm{Li}}^2 \overline{\langle h_z^2 \rangle} \tau, \tag{19}$$

which is valid in the fast motion limit (i.e., $\tau\gamma(\overline{\langle h_z^2 \rangle})^{1/2} \ll 1$) and the contribution to $1/T_2$ from nuclear dipole-dipole interactions is neglected. The contribution from nuclear dipolar interaction is of the order of 300 μs, so the above equation is valid only close to the zero-field T_g when it yields a T_2 value much smaller than 300 μs. The expression for $\langle h_z^2 \rangle$ is[56]

$$\langle h_z^2 \rangle = \sum_i \frac{\gamma_s^2 \hbar^2}{3 r_i^6} (1 - 3\cos^2\theta_i)^2 S(S+1). \tag{20}$$

Its average in Eq. (19) is estimated with the same numerical procedure as above and is found to be $(\overline{\langle h_z^2 \rangle})^{1/2}=0.12$ T. The value of τ above which the signal becomes again observable is $\tau \sim T_2 \sim 40$ μs $\gtrsim 1/(\overline{\langle h_z^2 \rangle})^{1/2}\gamma_{\mathrm{Li}}$.[29] In this slow motion regime, T_2 increases with increasing τ up to the limiting value given by the nuclear dipole-dipole interaction and the signal intensity is partially recovered as shown in Fig. 11 for the $H=1.1$ T data.

E. ^{11}B NMR

Figure 16 shows the ^{11}B NMR central $|I_z = -1/2\rangle \leftrightarrow |1/2\rangle$ transition spectra at applied magnetic fields $H=1.28$ and 4.7 T and $T=295$ K. The satellites from $|-3/2\rangle \leftrightarrow |-1/2\rangle$ and $|1/2\rangle \leftrightarrow |3/2\rangle$ transitions spread out due to anisotropic frequency shift since the measurements were performed on a powder sample and could not be detected due to limited signal to noise ratio.[56] The spectrum at $H=1.28$ T shows two peaks corresponding to the two singularities in the powder pattern of a second order quadrupole effect. The two peaks merge into one at $H=4.7$ T because the separation of the two peaks is inversely proportional to the field. If one assumes an axially symmetric EFG, then the separation of the two peaks ($\delta\nu$) is[56]

$$\delta\nu = \frac{25\pi}{24}\frac{\nu_Q^2}{H\gamma_{\mathrm{Li}}}, \tag{21}$$

where the quadrupole frequency ν_Q is

$$\nu_Q = \frac{3e^2qQ}{h2I(2I-1)} = \frac{1}{2}\frac{e^2qQ}{h},$$

$eq=V_{zz}$ is the electric field gradient along the axial symmetry axis, and Q and I are the quadrupole moment and spin of a ^{11}B nucleus, respectively. At $H=1.28$ T, $\delta\nu=44(4)$ kHz, so $\nu_Q=1.2(1)$ MHz. This value is close to that in crystalline B_2O_3 where $2\nu_Q=2.69\pm0.03$ MHz.[63] In both systems, boron atoms are at the centers of triangles with oxygen atoms at the vertices.

Since only the central line for ^{11}B ($I=3/2$) can be irradiated, the nuclear spin-lattice relaxation is intrinsically nonexponential. For a relaxation due to magnetic interactions, the recovery of the central line follows[64]

$$1 - \frac{M(t)}{M(\infty)} = C\exp(-2Wt) + (1-C)\exp(-12Wt), \tag{22}$$

where C depends on the saturation sequence and the degree of overlap of the satellite background with the central line and W is related to the transition rate $W_{m\to m-1}$ from the $|I_z=m\rangle$ to the $|m-1\rangle$ state through

$$W = \frac{W_{m\to m-1}}{(I-m+1)(I+m)} = \text{const},$$

where $m=\pm1/2$ or $3/2$ here. At low temperatures, due to the presence of a distribution of electronic spin relaxation times, Eq. (22) no longer fits the relaxation curves. We thus used the following phenomenological stretched exponential equation to fit the relaxation curves:

$$1 - \frac{M(t)}{M(\infty)} = C\exp[-(2W^*t)^\beta] + (1-C)\exp[-(12W^*t)^\beta]. \tag{23}$$

The saturation sequence we used consisted of nine $\pi/2$ pulses with a separation of 400 μs between neighboring pulses. The value of C is found to be in the range 0.3–0.4 at $H=4.7$ T and in the range 0.5–0.6 at $H=1.28$ T. The difference of the C values at the two fields is currently not understood.

The fitting results of W^* and β versus T at $H=1.28$ and 4.7 T are displayed in Fig. 17. The data displayed are only for $T\geqslant10$ K at $H=4.7$ T and $T\geqslant18$ K at $H=1.28$ T. Due to a loss of signal intensity (similar to ^{7}Li in the main panel of Fig. 11) and a large increase of relaxation rate, reliable W^* and β results cannot be obtained at lower temperatures. However, it is clear that ^{11}B NMR nuclear spin-lattice relaxation rates are also strongly enhanced at low temperature, in qualitative agreement with the slowing down of the spin fluctuations on approaching the zero-field spin-glass transition temperature.

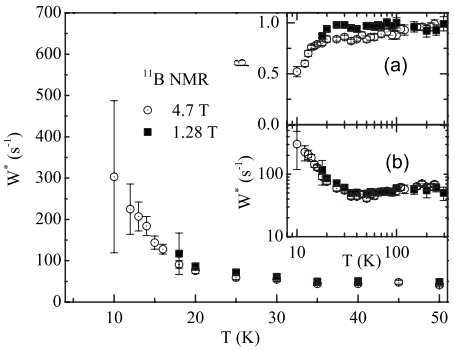

FIG. 17. W^* and β in Eq. (23) versus temperature T for ^{11}B NSLR at fields $H=1.28$ and 4.7 T. Main panel and inset (b): W^* versus T with different temperature scales. Inset (a): β versus T.

VI. SUMMARY AND CONCLUSIONS

X-ray diffraction studies on both single crystal and polycrystalline samples confirmed the previously reported structure of the $(Li_xV_{1-x})_3BO_5$ system. The structure contains both frustration and disorder, which are usually considered as necessary ingredients of a spin-glass system.

The high temperature magnetic susceptibility results cannot be explained by the simple picture of formation of VL1-VL4-VL1 linear trimers proposed in Ref. 27. The observed negative curvature in the inverse susceptibility below $T\approx100$ K might instead be due to the occurrence of magnetic clusters as the spin-glass transition temperature is approached. Magnetization measurements at low temperatures showed field-cooled and zero-field-cooled splitting of magnetization, slow relaxation of magnetization on a macroscopic time scale, and memory and rejuvenation effects which are all evidences of a spin-glass state below $T_g\sim10$ K.

The strong enhancement of nuclear spin-lattice relaxation rates upon approaching the zero-field T_g suggests that the dramatic slowing down of electronic spin dynamics persists even in a high field of 4.7 T where a true long range spin-glass transition may be suppressed as indicated by the magnetization measurements (Fig. 5). Our NMR measurements cannot distinguish whether the spin system is in the thermodynamic equilibrium or not at a particular temperature. In addition, we have no information on whether the spins freeze on a time scale longer than that of NMR ($\sim10^{-6}$ s).

We extracted the distribution of electronic spin relaxation times τ from NMR. A derived broad distribution of τ starts well above the zero-field spin-glass transition temperature T_g and becomes successively broader as the zero-field T_g is approached. The broad distribution of τ explains the observed loss of signal intensities displayed in the inset of Fig. 11. As illustrated in Fig. 15, as the temperature decreases toward T_g, more and more vanadium spins have τ in the range of $\sim10^{-10}$–10^{-6} s, which results in $T_2\lesssim40$ μs for the nearby ^{7}Li nuclear spins. Our modeling in terms of dynamical electronic spin heterogeneity[16,19–22,24] offers an alternative framework to models of homogeneous electronic relaxation.[18,15]

ACKNOWLEDGMENTS

We would like to thank B. J. Suh for helpful discussions. We also acknowledge A. Ellern in the molecular structure laboratory of Iowa State University for determining the structure of the single crystals through x-ray diffraction study. Work at the Ames Laboratory was supported by the Department of Energy, Basic Energy Sciences under Contract No. DE-AC02-07CH11358.

*Present address: Chemical Physics Program, Institute for Physical Science and Technology, University of Maryland, College Park, MD 20742.

[1] T. Nakamura and S. Endoh, J. Phys. Soc. Jpn. **71**, 2113 (2002).
[2] F. Matsubara, T. Shirakura, S. Endoh, and S. Takahashi, J. Phys. A **36**, 10881 (2003).
[3] K. Hukushima and H. Kawamura, Phys. Rev. B **72**, 144416 (2005).
[4] L. W. Lee and A. P. Young, arXiv:cond-mat/0703770v1 (unpublished).
[5] I. Campos, M. Cotallo-Aban, V. Martin-Mayor, S. Perez-Gaviro, and A. Tarancon, Phys. Rev. Lett. **97**, 217204 (2006).
[6] I. A. Campbell and H. Kawamura, arXiv:cond-mat/0703369v1 (unpublished); D. Ninomiya, T. Shirakura, Y. Iyama, and F. Matsubara, J. Magn. Magn. Mater. **310**, e512 (2007).
[7] D. S. Fisher and D. A. Huse, Phys. Rev. B **38**, 386 (1988).
[8] G. Parisi, Phys. Rev. Lett. **43**, 1754 (1979).
[9] J. Mattsson, T. Jönsson, P. Nordblad, H. Aruga Katori, and A. Ito, Phys. Rev. Lett. **74**, 4305 (1995).
[10] P. E. Jönsson, H. Takayama, H. A. Katori, and A. Ito, Phys. Rev. B **71**, 180412(R) (2005).
[11] P. E. Jönsson and H. Takayama, J. Phys. Soc. Jpn. **74**, 1131 (2005).
[12] G. G. Kenning, D. Chu, and R. Orbach, Phys. Rev. Lett. **66**, 2923 (1991).
[13] D. Chu, G. G. Kenning, and R. Orbach, Phys. Rev. Lett. **72**, 3270 (1994).
[14] D. Petit, L. Fruchter, and I. A. Campbell, Phys. Rev. Lett. **83**, 5130 (1999).
[15] D. Petit, L. Fruchter, and I. A. Campbell, Phys. Rev. Lett. **88**, 207206 (2002).
[16] A. P. Murani, J. Magn. Magn. Mater. **22**, 271 (1981).
[17] A. T. Ogielski, Phys. Rev. B **32**, 7384 (1985).
[18] C. Pappas, F. Mezei, G. Ehlers, P. Manuel, and I. A. Campbell, Phys. Rev. B **68**, 054431 (2003); K. Gunnarson, P. Svedlindh, P. Nordblad, and L. Lundgren, Phys. Rev. Lett. **61**, 754 (1988).
[19] L. Lundgren, P. Svedlindh, and O. Beckman, J. Magn. Magn. Mater. **25**, 33 (1981).
[20] L. E. Wenger, Lect. Notes Phys. **192**, 60 (1983).
[21] I. A. Campbell, A. Amoto, F. N. Gygax, D. Herlach, A. Schenck, R. Cywinski, and S. H. Kilcoyne, Phys. Rev. Lett. **72**, 1291 (1994); F. Matsukura and Y. Tazuke, J. Phys. Soc. Jpn. **63**, 1474 (1994).
[22] H. Takano and S. Miyashita, J. Phys. Soc. Jpn. **64**, 423 (1995).
[23] P. H. Poole, S. C. Glotzer, A. Coniglio, and N. Jan, Phys. Rev. Lett. **78**, 3394 (1997).
[24] S. C. Glotzer, N. Jan, T. Lookman, A. B. MacIsaac, and P. H. Poole, Phys. Rev. E **57**, 7350 (1998); K. Nemoto and H. Takayama, J. Phys. C **16**, 6835 (1983); C. Brangian, W. Kob, and K. Binder, J. Phys. A **35**, 191 (2002).
[25] A. Keren, G. Bazalitsky, I. Campbell, and J. S. Lord, Phys. Rev. B **64**, 054403 (2001).
[26] R. G. Palmer, D. L. Stein, E. Abrahams, and P. W. Anderson, Phys. Rev. Lett. **53**, 958 (1984).
[27] M. Onoda, J. Solid State Chem. **141**, 418 (1998).
[28] D. E. MacLaughlin and H. Alloul, Phys. Rev. Lett. **36**, 1158 (1976).
[29] D. E. MacLaughlin and H. Alloul, Phys. Rev. Lett. **38**, 181 (1977).
[30] D. A. Levitt and R. E. Walstedt, Phys. Rev. Lett. **38**, 178 (1977).
[31] D. Bloyet, E. Varoquaux, C. Vibet, O. Avenel, and P. M. Berglund, Phys. Rev. Lett. **40**, 250 (1978).
[32] M. C. Chen and C. P. Slichter, Phys. Rev. B **27**, 278 (1983).
[33] D. C. Johnston, S.-H. Baek, X. Zong, F. Borsa, J. Schmalian, and S. Kondo, Phys. Rev. Lett. **95**, 176408 (2005).
[34] J. Merrin, Y. Fudamoto, K. M. Kojima, M. Larkin, G. M. Luke, B. Nachumi, Y. J. Uemura, S. Kondo, and D. C. Johnston, J. Magn. Magn. Mater. **177-181**, 799 (1998).
[35] D. C. Johnston, Phys. Rev. B **74**, 184430 (2006).
[36] S. Kondo, D. C. Johnston, and L. L. Miller, Phys. Rev. B **59**, 2609 (1999).
[37] B. H. Toby, J. Appl. Crystallogr. **34**, 210 (2001).
[38] A. C. Larson and R. B. Von Dreele, Los Alamos National Laboratory Report No. LAUR 86-748, 2004 (unpublished).
[39] J. B. Goodenough, *Magnetism and the Chemical Bond* (Interscience, New York, 1963).
[40] J. B. Goodenough, Phys. Rev. **117**, 1442 (1960).
[41] R. Omari, J. J. Prejean, and J. Souletie, J. Phys. (Paris) **44**, 1069 (1983).
[42] P. W. Selwood, *Magnetochemistry*, 2nd ed. (Interscience, New York, 1956).
[43] B. Southern, J. Phys. C **8**, L213 (1975).
[44] M. M. Zaripov, V. S. Kropotov, L. D. Livanova, and V. G. Stepanov, Dokl. Akad. Nauk SSSR **173**, 1043 (1967).
[45] D. C. Johnston, T. Saito, M. Azuma, M. Takano, T. Yamauchi, and Y. Ueda, Phys. Rev. B **64**, 134403 (2001).
[46] Y. Ueda, J. Kikuchi, and H. Yasuoka, J. Magn. Magn. Mater. **147**, 195 (1995).
[47] A. P. Ramirez, Annu. Rev. Mater. Sci. **24**, 453 (1994).
[48] G. Griffith, F. A. Volkening, and H. Claus, J. Appl. Phys. **57**, 3392 (1985).
[49] K. Binder and A. P. Young, Rev. Mod. Phys. **58**, 801 (1986).
[50] J. Ferré, M. Ayadi, R. V. Chamberln, R. Orbach, and N. Bontemps, J. Magn. Magn. Mater. **54-57**, 211 (1986).
[51] R. V. Chamberlin, G. Mozurkewich, and R. Orbach, Phys. Rev. Lett. **52**, 867 (1984).
[52] Y. Sun, M. B. Salamon, K. Garnier, and R. S. Averback, Phys. Rev. Lett. **91**, 167206 (2003).
[53] F. Lefloch, J. Hammann, M. Ocio, and E. Vincent, Europhys. Lett. **18**, 647 (1992).

[54] M. Sasaki, P. E. Jönsson, H. Takayama, and P. Nordblad, Phys. Rev. Lett. **93**, 139701 (2004).
[55] E. Fukushima and S. B. W. Roeder, *Experimental Pulse NMR: A Nuts and Bolts Approach* (Perseus Books, Cambridge, 1981).
[56] A. Abragam, *Principles of Nuclear Magnetism* (Oxford University Press, Oxford, 1982).
[57] J. A. Ibers, C. H. Holm, and C. R. Adams, Phys. Rev. **121**, 1620 (1961).
[58] H. M. McConnell and R. E. Robertson, J. Chem. Phys. **29**, 1361 (1958).
[59] M. Belesi, A. Lascialfari, D. Procissi, Z. H. Jang, and F. Borsa, Phys. Rev. B **72**, 014440 (2005).
[60] T. Moriya, Prog. Theor. Phys. **16**, 23 (1956).
[61] F. Borsa and A. Rigamonti, in *Magnetic Resonance of Phase Transitions*, edited by F. J. Owens, C. P. Poole, and H. A. Farach (Academic, New York, 1979), p. 103.
[62] C. P. Slichter, *Principles of Magnetic Resonance* 3rd ed. (Springer, Berlin, 1990).
[63] C. Rhee and P. J. Bray, J. Chem. Phys. **56**, 2476 (1972).
[64] E. R. Andrew and D. P. Tunstall, Proc. Phys. Soc. London **78**, 1 (1961).